LAMINAR FLOW CONTROL ALONG THE ATTACHMENT LINE OF A SWEPT WING

Jeanne Methel, Fabien Méry, Maxime Forte, and Olivier Vermeersch

ONERA/DMPE
Université de Toulouse
F-31055 Toulouse, France
e-mail: jeanne.methel@onera.fr, fabien.mery@onera.fr

Key words: laminar-turbulent transition, attachment line contamination, wall suction

Abstract. Reducing aircraft fuel consumption by maximising the extent of laminar flow on wings assumes that the initial flow, along the wing's attachment line, is laminar. However, if the wing is attached to a solid wall, the wing's attachment line can be contaminated by the turbulent boundary layer developing over the solid wall for flow conditions summarised in a critical Reynolds number ($\overline{R}$) greater than 250. Since typical $\overline{R}$ values encountered in flight can be well above 400, techniques, such as wall suction along the wing's leading edge were developed to further delay the threshold $\overline{R}$ at which contamination occurs. The present paper presents the results from an experimental investigation performed on the ONERA DTP-A model fitted with leading edge suction capabilities. The experiment was performed in the ONERA F2 wind tunnel in the framework of the EU-funded Clean Sky 2 HLFC-WIN project (LPA-IADP platform), while the suction panels were manufactured by Aernnova, an aero-component manufacturing company. Hot film measurements and infra-red thermography showed that attachment line contamination could effectively be delayed up to threshold $\overline{R}$ values of 1000 for large suction flow rates. Although panels from different manufacturing processes and with different geometric characteristics were tested, no significant difference from these parameters were observed.

1 INTRODUCTION

Promoting laminar flow over the wings and empennage of an aircraft can result in a significant reduction in skin-friction drag, and consequently, fuel consumption. Although many techniques were successfully developed to maximise laminar flow, all work under the assumption that the initial starting flow, also known as the attachment line, is laminar. More precisely, the attachment line is defined at the streamline in the leading edge region across which flow separates between the upper and the lower surfaces, and where static pressure reaches a maximum.

Assuming laminar flow at the attachment line is not guaranteed, especially in the case where the wing section is attached to a solid wall (e.g., fuselage or wind tunnel wall). In this type of configuration, the turbulence that develops over the solid wall can propagate along the attachment line, resulting in attachment line contamination and turbulent flow over the entire wing. The contamination process is highly non-linear in that, once relevant flow conditions are reached, the attachment line as well as the entire wing become fully turbulent quasi-instantaneously.

Theoretical and experimental investigations by Pfenninger [1] and Poll [2] enabled to define a criterion, critical Reynolds number $\overline{R}$ equal to 250, above which attachment line contamination (ALC) is most likely to occur. This Reynolds number is defined as:

$$\overline{R} = \frac{W_e \eta}{\nu} \quad \text{with} \quad \eta = \sqrt{\frac{\nu}{\frac{dU_e}{dx}\big|_{x=0}}},\tag{1}$$

where W_e is the spanwise component of velocity defined as $W_e = Q_\infty \sin\phi$, Q_∞ the freestream velocity, ϕ the wing's sweep angle, ν the kinematic viscosity, and η a parameter related to the gradient of velocity in the curvilinear abscissa in the chordwise direction at the location of the attachment line, i.e., $x = 0$. The schematic representation of the contamination process shown in Figure 1 also illustrates the used nomenclature. Since $\overline{R}$ values encountered in flight by commercial aircraft are typically much greater than 400, avoiding ALC is therefore necessary to consider the implementation of laminar wings.
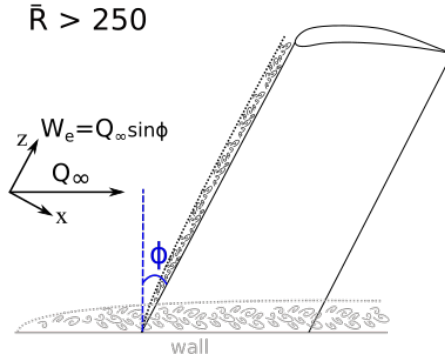

Figure 1: Schematic representation attachment line contamination with nomenclature.

One proven approach in preventing attachment line contamination is to use Laminar Flow Control (LFC) such as wall suction through micro-perforated panels at the leading edge of the wing. Direct numerical simulations performed by [3] initially showed the ability of wall suction to delay contamination up to threshold $\overline{R}$ values of 400, while later experimental investigations by [4], [5] showed that this limit could be pushed even further, at approximately 650. In the present paper, references to the critical $\overline{R}$ always correspond to the range 250-280; while the threshold $\overline{R}$ is the value for which contamination occurs in the presence of active flow control, and is therefore generally greater than the critical $\overline{R}$.

Once contamination is cancelled and if freestream turbulence is low, then natural transition in both the spanwise and chordwise (z- and x-, respectively) directions can occur. In both cases, transition can be modelled by linear stability theory, where the primary instabilities of the boundary layer evolve linearly up to a certain amplification threshold, past which secondary instabilities appear. At this stage, the first turbulent spot quickly occurs, heralding the beginning of the laminar-turbulent transition region and the breakdown to turbulence. For attachment line transition along the spanwise direction, the primary instabilities are known as Görtler-Hämmerlin. In the chordwise direction, the primary instabilities can take the form of

either crossflow instabilities closer to the leading or Tollmien-Schlichting instabilities further downstream.

The present investigation aimed at testing the same model used in the experiments described in [4], [5] at higher $\overline{R}$ values to further test the limits of suction in delaying contamination. Another objective was to study the effect of the micro-perforated panels' geometric parameters on the effectiveness of wall suction. First, an overview of the experimental set-up will be provided, describing the wind tunnel facility, model and instrumentation. Next the experimental results will be discussed: first, by examining the pressure coefficient distribution at the leading edge and introducing the concept of the effective sweep angle; next by validating all tested configurations without wall suction against the Poll and Pfenninger criterion; and finally, by examining the evolution of the threshold $\overline{R}$ values where contamination occurs as a function of wall suction and the micro-perforated panel characteristics.

2 EXPERIMENTAL SET-UP

In this section, the experimental set-up is described, including the wind tunnel test facility and model used, the micro-perforated suction panels manufactured for this investigation, and the instrumentation available to transition or contamination monitoring.

2.1 Experimental facility and model

Experiments were performed in the ONERA F2 wind tunnel facility, a subsonic atmospheric closed-loop wind tunnel with a rectangular test section (1.8 m high x 1.4 m wide at the entrance). Over the 5 m length of the test section, the floor and ceiling diverge by 0.45° to account for the wall boundary layers. The freestream velocities achievable by the wind tunnel with the large model used for this experiment range from $5\,\mathrm{m\,s^{-1}}$ and $85\,\mathrm{m\,s^{-1}}$. Turbulence levels are low enough to allow for natural laminar-turbulent transition experiments.

The DTP-A model used during this experimental was specifically designed to study attachment line transition and contamination. As shown on Figure 2a), the model consists of a semi-cylindrical leading edge with a radius of 200 mm extended by straight side panels forming a triangular cross-section. The total chord length, defined in the normal direction with respect to the leading edge, is 1200 mm. The model is mounted vertically (Figure 2b)) and is attached to the floor of the test section. In Figure 2c), the model is at a geometric sweep angle of 50°; subsequently, to reach higher Reynolds numbers $\overline{R}$, the model was also set to ϕ equal to 60°. As a note, during the past experiments in [5] performed during the winter 2018-2019, only the 50° sweep configuration was tested.

2.2 Micro-perforated suction panels

Along the leading edge of the model, three suction chambers sealed by a micro-perforated titanium panel can be seen on Figure 2. The panels were perforated and shaped to match the leading edge curvature by the manufacturer Aernnova, a company specialised in the design and manufacturing of aerostructures and components in the aerospace industry, and its affiliates. An overview of the panel geometries tested over the past two test campaigns in 2018 and 2022 is provided in Table 2.2. Only panel P1 was tested during both campaigns for repeatability validation between wind tunnel tests, and the present paper will focus on panels P4 and P5.
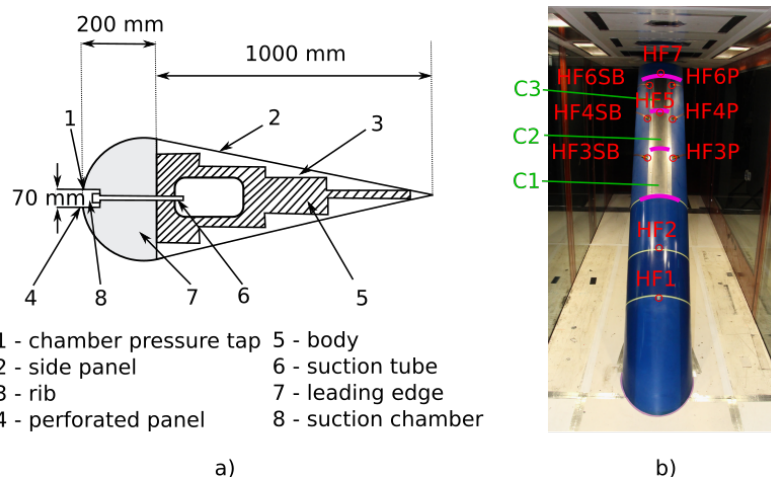
Figure 2: DTP-A model a) cross-section with key geometric features and dimensions, and b) front view of the model mounted inside the test section.

Table 1: Summary of the micro-perforated suction panel geometry tested over the last two test campaigns. Panel P1 was tested during the 2022 campaign for repeatability validation. Panels P2 and P3 shown in italic were not tested in 2022.

	Hole Ø [µm]	Pitch [µm]	Geometric porosity [%]	ΔP at $\dot{m}$=10 g s^{-1} [Pa]
2022 test campaign				
P4	60	590	0.8	11000
P5	60	485	1.2	4500
2018 test campaign				
P1	50	500	0.8	4800
P2	*130*	*1820*	*0.4*	*7400*
P3	*50*	*700*	*0.4*	*13500*

In particular, panel P4 was designed to have almost equivalent geometry as panel P1, with a slight increase in hole diameter from 50 µm to 60 µm, to investigate the effect of manufacturing process between the two dates. Next, panel P5 was designed to study the effect of increasing porosity on suction performance, compared to panel P4.

All panel perforations had a square pattern so that the geometric porosity, generally defined as the open area over the total area, is the area of the hole over the squared pitch distance. Additionally, geometric porosity is provided, as opposed to a more physical porosity related to the pressure loss across the panel. In particular, when comparing panels P1 and P4, which were designed to have the same geometric porosity, their pressure losses are different: for a suction mass flow rate of 10 g s^{-1} across each three suction chambers, panel P1 results in a 4500 Pa pressure loss, as opposed to P4 with a 11 000 Pa, as shown in Table 2.2 and Figure 3. This difference in pressure loss cannot solely be attributed to the slight change in hole diameter, but also to the difference in manufacturing process.

Inspection of the panel geometries using an Alicona Infinite Focus SL 3D optical surface

measurements allowed to determine that both pitch and diameter dimensions were within $\pm$ 5 μm of specifications. Although such variation in the pitch only results in a $\pm0.02\%$ variation in geometric porosity, the same variation in hole diameter results in a $\pm0.15\%$ variation in porosity, which, relative to the low porosities under consideration, is significant. The geometric porosity should therefore be considered more as an ideal specification for manufacturing requirements, while the pressure loss across the panel for various suction flow rates should be considered the relevant parameter of interest.

As can be seen from Figure 3, although panels P1 and P5 have different hole pitch and diameter, their pressure loss across the different suction flow rates are comparable, as opposed to panel P4 that induces much greater pressure losses at high suction flow rates. Another suction parameter of interest that will be used subsequently in this paper is the ideal suction velocity, defined as:

$$V_p = \frac{\dot{m}}{\rho A_{\text{panel}}} \tag{2}$$

with $\dot{m}$ the suction mass flow rate, ρ the air density evaluated closest to the suction chamber, and A_{panel} the suction panel total surface area.
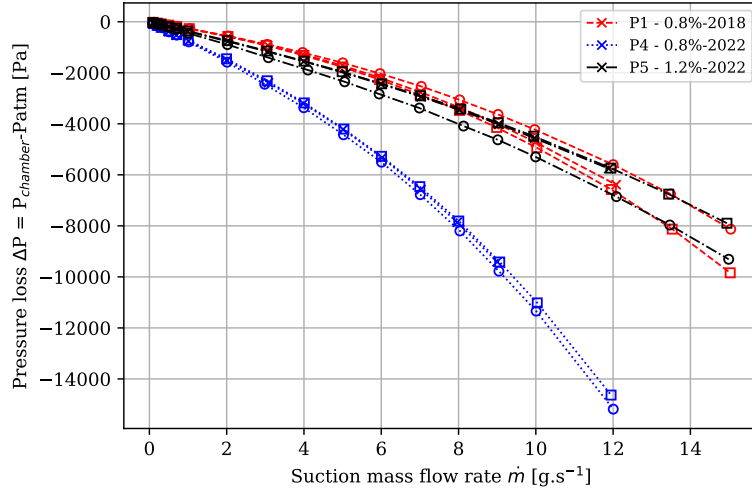

Figure 3: Pressure loss (without freestream flow) as a function of suction mass flow rate for all three suction panels investigated in 2022. Each symbol corresponds to one of the suction chambers (cross: chamber 1, square: chamber 2, and circle: chamber 3.

2.3 Instrumentation

Four lines of static pressure ports, shown as the magenta lines on Figure 2b), are located at the junction between the different suction chambers (at the beginning of chamber C1, between C1 and C2, between C2 and C3, and at the end of C3), and spanning at least the entire width of the suction chambers. Since the model was set at a zero-lift angle of attack, the static pressure

ports allowed to verify that flow symmetry was achieved. The pressure taps are orthogonal to the leading edge, i.e., aligned with the chordwise x-direction.

To monitor the attachment line contamination or natural transition in the leading edge region, hot films were also mounted on the model, as shown by the red circles on Figure 2b). Four of them were located along the attachment line: two upstream of the suction region, and closest to the junction with the test section floor, HF1 and HF2; one at the junction between chambers C2 and C3, HF5; one downstream of C3, HF7. Then, two hot films were placed downstream (in the x-direction) of each of the three suction chambers, as shown on Figure 2b) by the red labels, with "SB" (resp. "P") corresponding to the "starboard" (resp. "port") side. Hot films could not be placed over the perforated panels without blocking a portion of the suction area, and would have made changing the different panels more difficult. Additionally, since contamination is such an abrupt phenomenon involving the entire model quasi-instantaneously, the hot films' shifted location with respect to the attachment line should not be significant enough to affect the threshold $\overline{R}$ detection. Finally, by having two hot films on either side of each suction chamber, flow symmetry can also be further validated.

Infra-red (IR) thermography was also used to monitor contamination and transition. Since the leading edge, outside the suction chambers, consists of polyurethane, IR measurements could be performed directly on the model surface without the need for additional modifications or inserts. Two IR cameras (IRCAMERA IRC906 and FLIR SC7650) were mounted so as to be flush with the test section ceiling and to cover the entire span of the suction region down to the hot film second closest to the floor along the attachment line.

Finally the suction flow rate was set using an electric side channel vacuum pump and monitored using Brooks 5863S thermal mass flow meters. Manual valves were used to modify the flow rate during testing and were balanced to within $0.1\,\mathrm{g\,s^{-1}}$ of one another.

3 EXPERIMENTAL RESULTS

In this section the experimental results are first discussed in terms of the pressure coefficient distributions to allow the introduction of the notion of the effective sweep angle. Next the experimental set-up is validated for both configurations (at geometric sweep angles 50° and 60°) in the no suction case. Finally, the effect of wall suction in delaying the threshold $\overline{R}$ at which contamination occurs is compared for all three suction panels, as well as with previous experimental investigations performed in the same wind tunnel and on the same model.

3.1 Pressure coefficient distribution and effective sweep angle

Given its geometry and flow regime of investigation, the DTP-A model can be approximated as an infinite swept cylinder in inviscid flow. Under this assumption, the pressure coefficient C_p around a swept cylinder of radius r can be expressed in terms of the azimuthal angle θ (related to the curvilinear abscissa in the chordwise direction x such that $\theta = x/r$):

$$C_p(\theta) = \cos^2 \phi (1 - 4\sin^2 \theta) \tag{3}$$

At the leading edge, where θ is zero, the C_p value should be maximum. In order to match the C_p in the inviscid flow solution at the leading edge with the measured C_p, an effective sweep angle ϕ_{eff} is introduced and defined such that:

$$\phi_{\text{eff}} = \cos^{-1} \sqrt{\max\left(C_{\text{p,exp}}\right)} \tag{4}$$

The measured pressure coefficient distributions along the different spanwise positions of the model are shown in Figure 4 for both sweep angle configurations at freestream velocity Q_∞ equal to $50\,\text{m s}^{-1}$. On Figure 4a), all $C_{\text{p,exp}}$ distribution overlap relatively well: the ϕ_{eff} angle of $57°$ (shown as the dashed line) in this case is chosen as the mean value across all four maximum $C_{\text{p,exp}}$. As an illustration, the theoretical pressure coefficient distributions calculated using equation 3 with both the geometric and effective sweep angles are shown as the dotted and dashed lines respectively.

However, in the case of the $60°$ geometric sweep angle configuration, a spanwise evolution of the $C_{\text{p,exp}}$ is observed. Based on flow visualisation performed using coloured viscous film showed no signs of significant recirculation regions on the DTP-A model. A numerical investigation is ongoing to provide further explanations for this phenomenon. Given the spanwise evolution of the $C_{\text{p,exp}}$, a conservative approach to determine the ϕ_{eff} was chosen. The static pressure line 1 was used to determine ϕ_{eff} value of $70°$ and will be used in all subsequent calculations of $\overline{R}$.
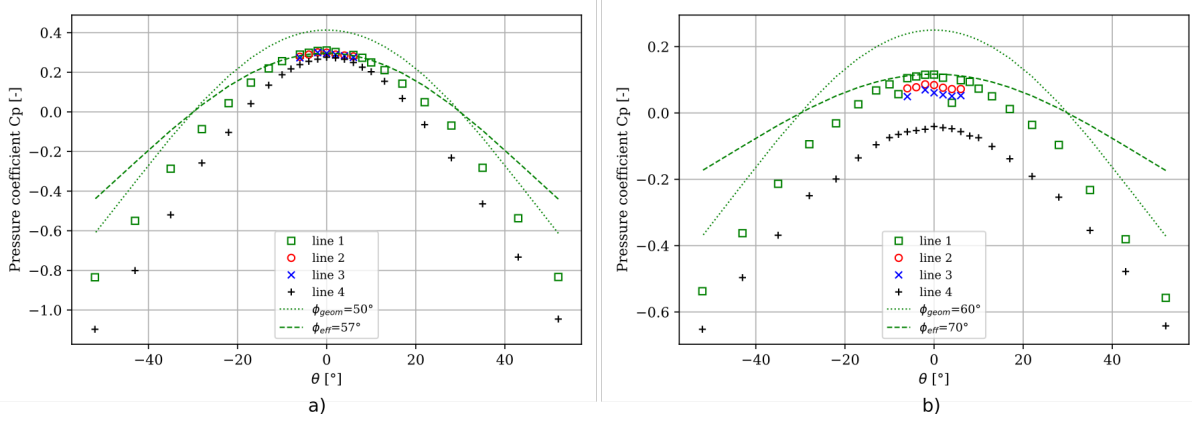

Figure 4: Pressure coefficient distribution on the different static pressure lines along the spanwise direction for Panel P5 with no suction at $Q_\infty = 50\,\text{m s}^{-1}$. a) $\phi_{\text{geom}} = 50°$ and b) $\phi_{\text{geom}} = 60°$

Given the infinite sweep cylinder assumption and the use of ϕ_{eff}, equation 1 for $\overline{R}$ can be further simplified to take the form of:

$$\overline{R} = \sqrt{\frac{Q_\infty D}{2\nu} \frac{\sin\phi_{\text{eff}} \tan\phi_{\text{eff}}}{2}} \tag{5}$$

with $D = 2r$ the diameter at the leading edge.

3.2 Validation of the contamination criteria without suction

The first step before investigating the effect of wall suction as an active anti-contamination device is to verify that the reference condition for both sweep configurations agree with the critical $\overline{R} = 250$ criterion established by Pfenninger [1] and Poll [2]. Based on equation 5, $\overline{R}$ is modified by varying the freestream velocity Q_∞ for a given sweep angle configuration.

Figure 5 shows the evolution of voltage fluctuations in terms of Root Mean Square (RMS) for all hot films as a function of $\overline{R}$ for both sweep configurations and without wall suction. The threshold contamination $\overline{R}$ value corresponds to the value at which fluctuations start to increase abruptly: no indication of the imminence of contamination can be detected before its occurrence. On Figure 5a), the first observation is that all hot films, except those identified as HF1 and H2, show an abrupt increase in voltage fluctuations at critical $\overline{R}$ equal to 275 ±15 and for all suction panels. These hot films signals therefore confirm that even though some of the hot films (HF3SB, HF3P, HF4SB, HF4P, HF6SB and HF6P) are slightly offset from the attachment line itself, their signal is still useful to identify the onset of contamination. Additionally, no effect from the suction panels without suction can be observed. The critical $\overline{R}$ value is within the range defined by Pfenninger and Poll, indicating that the experimental set-up is appropriate for the investigation of attachment line contamination.

The signals from HF1 and HF2 have greater RMS levels starting from the first $\overline{R}$ value, which corresponds to the minimum freestream velocity achievable by the wind tunnel facility. These hot films, located closest to the model/floor junction, are actually located inside the floor's turbulent boundary layer. Their signals therefore are not an indication of the attachment line boundary layer regime, and will not be used.

Figure 5b) shows the same measurements for the ϕ_{geom} equal to 60° configuration. Combining the higher sweep angle and the minimum achievable freestream velocity, the minimum $\overline{R}$ value attained is equal to 300. However, considering the RMS levels as well as comparing the general trend with that of the ϕ_{geom} equal to 50° configuration, contamination has occurred at a value close to or below 300, close to the reference empirical criterion.
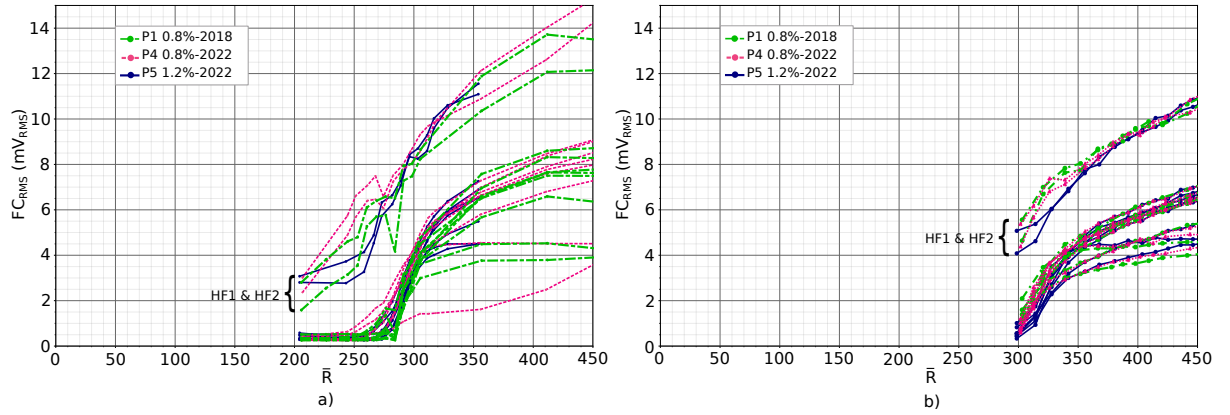

Figure 5: Voltage fluctuations of all hot films for all suction panels without wall suction. a) $\phi_{\text{geom}} = 50°$ and b) $\phi_{\text{geom}} = 60°$.

Both sweep angle configurations without wall suction therefore provide a sound reference, in agreement with the literature on contamination in low freestream turbulence. Since the two hot films HF1 and HF2, closest to the wall/model junction, are known to be always in the test section floor's boundary layer, their signal will not be used subsequently to determine the threshold $\overline{R}$. On the other hand, since all other hot films seem to answer quasi-instantaneously,

their signals will be used and compared with one another to check for any lag in the spanwise spread of contamination.

3.3 Anti-contamination using wall suction

Once the reference configurations are validated, wall suction along the model leading edge could then be applied to investigated the delay of contamination as a function of suction velocity.

Qualitatively, infra-red thermography images are shown on Figure 6 to illustrate the effect of applying wall suction at $\overline{R}$ values well above the contamination threshold without any control.

On Figure 6a), the DTP-A model at a geometric sweep angle of 50° and with a suction velocity V_p of $21\,\mathrm{cm\,s^{-1}}$ over panel P5 (1.2%-2022) is shown at an $\overline{R}$ equal to 575, which corresponds to a freestream velocity Q_∞ of $40\,\mathrm{m\,s^{-1}}$. As indicated in the figure caption, for this case, the laminar flow regions appear in light gray. The camera is fixed over the end of chamber C2 and the entire surface of C3, and the small bright spots followed by a dark gray turbulence cone correspond to the hot films located downstream of the suction chambers. With this suction flow rate, contamination is avoided and natural transition along the chordwise direction can take place, although its position is outside the camera's view.

Next, Figure 6b) shows the same view at a higher $\overline{R}$ equal to 610, which corresponds to Q_∞ equal to $50\,\mathrm{m\,s^{-1}}$. In this case, although contamination is still cancelled, the natural transition front starts to appear. The visible sawtooth pattern, especially at the top of chamber C3 near the sides of the leading edge, is characteristic of the crossflow transition mechanism for swept wings. Finally, in Figure 6c), contamination is avoided at a still higher $\overline{R}$ value of 670, corresponding to Q_∞ equal to $55\,\mathrm{m\,s^{-1}}$, while the crossflow transition front moves further upstream, closer to the leading edge, due to the greater freestream velocity.

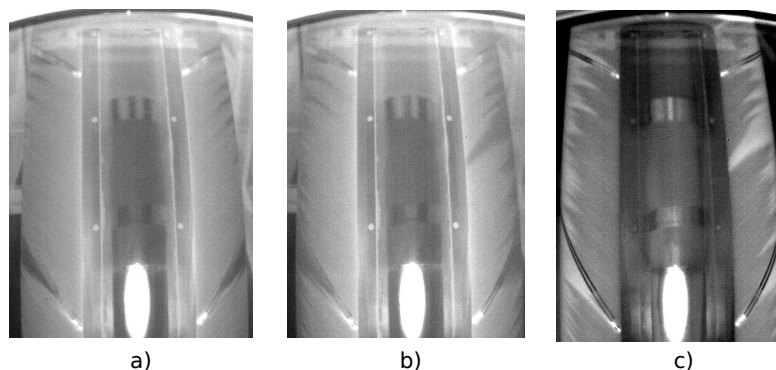a)   b)   c)

Figure 6: Infra-red thermography showing a cross-flow transition pattern of panel P5 (1.2%-2022) for configuration $\phi_{\mathrm{geom}} = 50°$ and $\phi_{\mathrm{eff}} = 57°$ with suction velocity $21\,\mathrm{cm\,s^{-1}}$ at a) $\overline{R} = 575$, b) $\overline{R} = 610$, and c) $\overline{R} = 670$. Note that for figures a) through b), laminar regions are light gray whereas for c) laminar regions are dark gray due to a change in freestream flow temperature to recover thermal desequilibrium with the model and enhance IR visualisations.

Next, a quantitative assessment of the effectiveness of leading edge wall suction using the hot films signals is provided in Figure 7. Similar to Figure 5, the voltage fluctuations in RMS are shown as a function of $\overline{R}$ (modified by changing the freestream velocity for each sweep

configuration). For each suction velocity shown by a different colour, the signals from both hot films HF6SB and HF6P are shown: up to suction velocities of $30\,\mathrm{cm\,s^{-1}}$, both hot films show an abrupt increase in their RMS values at the same $\overline{R}$, indicating symmetric flow across the attachment line. On Figure 7b) however, the case with suction velocity $37\,\mathrm{cm\,s^{-1}}$ is not symmetric and the threshold $\overline{R}$ is different depending on the hot film.

Regardless of the sweep configuration, increasing suction flow velocity across panel P5 consistently delayed the threshold $\overline{R}$. However, although a delay of 100 units of $\overline{R}$ was achieved by going from the no suction to the $3\,\mathrm{cm\,s^{-1}}$ case, the threshold $\overline{R}$ was only delay by 40 units when going from $21\,\mathrm{cm\,s^{-1}}$ to $24\,\mathrm{cm\,s^{-1}}$. Increasing suction velocity therefore seems to become less effective at higher $\overline{R}$. The same results were found for panels P1 and P4.

One noticeable trend for suction velocities above $12\,\mathrm{cm\,s^{-1}}$ is the gradual increase in RMS value preceding the abrupt boost, indicative of contamination. This initial intermediate increase is actually characteristic of the crossflow instabilities developing over the hot films, and should therefore not be interpreted as a phenomenon related contamination.
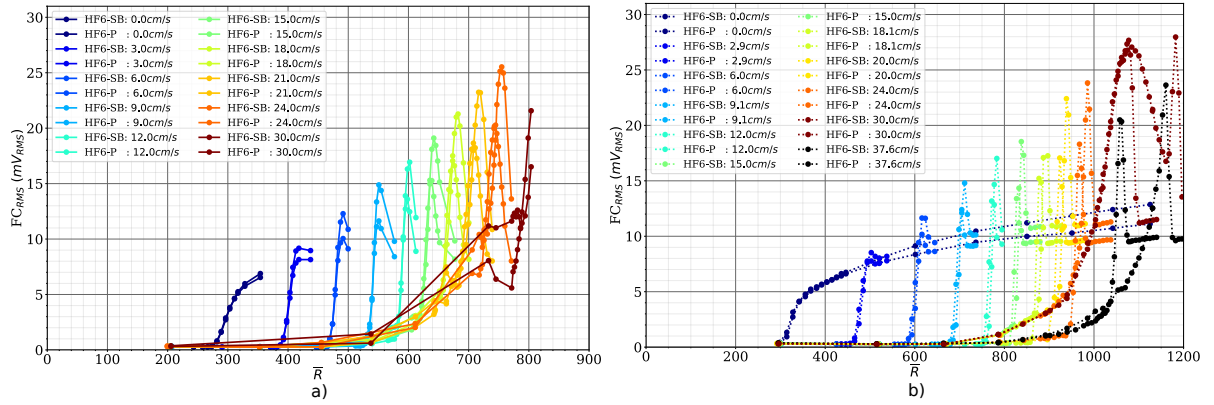

Figure 7: Voltage fluctuations of hot films HF6-SB (starboard) and HF6-P (port) for panel P5 1.2% - 2022 for all tested suction velocities at a) $\phi_{\mathrm{geom}} = 50°$ and $\phi_{\mathrm{eff}} = 57°$ and b) $\phi_{\mathrm{geom}} = 60°$ and $\phi_{\mathrm{eff}} = 70°$.

A more concise representation to relate the delay in threshold $\overline{R}$ due to wall suction is to use the non-dimensional suction parameter K, defined as:

$$K = \frac{V_p \overline{R}}{Q_\infty \sin \phi}. \tag{6}$$

In this expression, V_p is negative when applying suction, and therefore K will also be negative. Figure 8 shows the evolution of the threshold $\overline{R}$ detected using either HF6P or HF6SB as a function of K for all suction panels and sweep angle configurations. Overlaid with the experimental data, the dashed line is the empirical correlation $\overline{R} = 250 - 150K$ established by Arnal et al. in [4].

Regardless of suction panel or sweep angle configuration, all data points for both hot films agree well with the empirical correlation. The only main discrepancy between the two hot films is for suction velocity $37\,\mathrm{cm\,s^{-1}}$, corresponding to K close to -7 for HF6P. This asymmetry
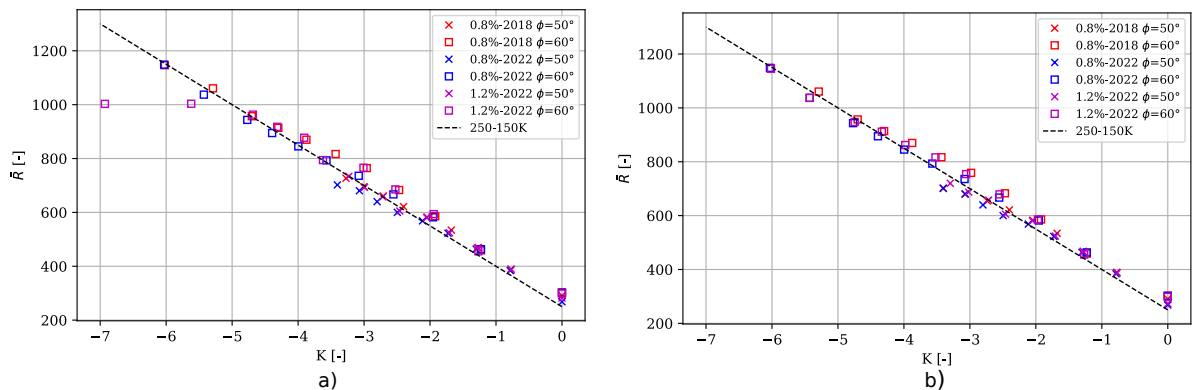
Figure 8: Evolution of threshold $\overline{R}$ as a function of non-dimensional suction parameter K for all suction panels and sweep angle configurations evaluated at a) hot film HF6P and b) hot film HF6SB to check for symmetry.

was already identified in Figure 7. Overall though, increasing suction can effectively delay the threshold $\overline{R}$ up to values as high as 1000, relevant to commercial aircraft flight envelope.

4   CONCLUSIONS

Assuming laminar flow at the attachment line of a wing section attached to a solid wall or fuselage is not guaranteed and can completely cancel downstream strategies to maintain laminar flow. In particular, the incoming turbulent boundary layer from the solid wall can contaminate the wing section attachment line boundary layer and therefore the entire wing. The critical value of the Reynolds number $\overline{R}$ above which transition is likely to occur is between 250 and 280, while typical $\overline{R}$ values encountered in flight by commercial aircraft are significantly greater than 400. For this reason, strategies to delay the contamination threshold have to be adopted to consider the implementation of laminar wings in commercial aviation.

One effective strategy is by applying wall suction through micro-perforated panels located on the leading edge of the wing section. Although previous experiments confirmed that this method allowed to push the threshold $\overline{R}$ to 650, limitations inherent to previous experimental set-ups prevented verifying if greater threshold $\overline{R}$ values could be achieved. For this reason, the present paper focused on testing the DTP-A model at two sweep angle configurations in order to reach greater $\overline{R}$ values. Suction panels with varying geometries and from different manufacturing processes were tested. Both IR thermography and hot film anemometry were used to monitor the boundary layer in the leading edge region. Based on these measurements, wall suction was found to effectively delay the threshold $\overline{R}$ to value beyond 1000. The effect of panel geometry or manufacturing process was not significant in affecting suction effectiveness.

Future work on this topic within the HLFC-WIN project involves testing anti-contamination using suction in the compressible flow regime at the ONERA wind tunnel facility S1MA, again with suction panels manufactured by Aernnova. More generally, it will be necessary to investigate the feasibility of such high suction flow velocities using a practical suction system that could be mounted in a commercial aircraft wing or empennage.

5   ACKNOWLEDGMENTS

REFERENCES

[1] Pfenninger, W., Flow phenomena at the leading edge of swept wings. Recent development in boundary layer research. *AGARDograph 97, Part IV* (1965).

[2] Poll, D., Some aspects of the flow near a swept attachment line with particular reference to boundary layer transition. *College of Aeronautics, Cranfield Institute of Technology* (1978).

[3] Spalart, P.R., Direct numerical study of leading-edge contamination. *Fluid dynamics of three-dimensional turbulent shear flows and transition* 1-5 (1989)

[4] Arnal, D. and Juillen, J.-C. and Reneaux, J. and Gasparian, G., Laminar Flow Control along the wing leading edge. *Aerospace Science and Technology* 1(8):505–517 (1997)

[5] Méry, F. and Vermeersch, O. and Forte, M., Laminar Flow control along the wing leading edge. *1st Aerospace Europe Conference AEC2020* (2020).